

The dipole cross section by the unintegrated gluon distribution at small x

G.R.Boroun*

Department of Physics, Razi University, Kermanshah 67149, Iran
(Dated: May 26, 2023)

We apply a previously developed scheme to consistently include the improved saturation model for the unintegrated gluon distribution (UGD) in order to evaluate, in the framework of k_t factorization, at small x at the next-to-leading order (NLO) in α_s . We start the unintegrated gluon distribution with a parametrization of the deep inelastic structure function for electromagnetic scattering with protons, and then extract the color dipole cross section, which preserves its behavior success in a wide range of k_t^2 in comparisons with the UGD models (M. Hentschinski, A. Sabio Vera and C. Salas (HSS), I.P.Ivanov and N.N.Nikolaev (IN) and G. Watt, A.D. Martin and M.G. Ryskin (WMR)). These results show that the geometric scaling holds for the improved saturation model in a wide kinematic region rQ_s , and are comparable with the Golec-Biernat-Wüsthoff (GBW) model. The unintegrated gluon distribution at low and high momentum transfer in a wide range of x is considered.

I. Introduction

Although our knowledge of the proton structure at small- x is very limited, novel opportunities will be opened at new-generation facilities (Electron-Ion Collider(EIC), High-Luminosity Large Hadron Collider (HL-LHC), Forward Physics Facility (FPF)). Combining the information coming from dipole cross sections and p_T -unintegrated densities could play an important role. In particular, polarized amplitudes and cross sections for the exclusive electroproduction of ρ and ϕ mesons at the Hadron-Electron Ring Accelerator (HERA) and the EIC are very sensitive to the unintegrated gluon distribution (UGD) model adopted, whereas forward Drell-Yan dilepton distributions at the Large Hadron Collider beauty (LHCb) are very sensitive to next-to-leading logarithmic corrections. Indeed, the dipole cross section is directly connected via a Fourier transform to the small- x UGD, whose evolution in x is regulated by the Balitsky-Fadin-Kuraev-Lipatov (BFKL) equation [1]. The BFKL equation retains the full Q^2 dependence and not just the leading $\ln Q^2$ terms. Indeed the resummation of terms is proportional to $\alpha_s \ln(1/x)$ to all orders. This involves considering this means that we do not have strongly ordered k_t but instead integrate over the full range of k_t in phase space of the gluons [2,3]. The BFKL equation governs the evolution of the UGD, where the k_t -factorization is used in the high energy limit in which the QCD interaction is described in terms of the quantity which depends on the transverse momentum of the gluon [4]. In the k_t -factorization framework, the gluon distribution depends on x and k_t^2 , where x and k_t^2 being the fractional momentum of proton carried by gluon and the transverse momentum of gluon respectively. At high energies, the k_t -factorization is a suitable formalism to compute the relevant distribution and cross sections. Within this regime, the longitudinal momentum fraction of partons, x , is small. The unintegrated gluon distribution function is thus of great phenomenological and theoretical interest to develop the formalism which includes the transverse momentum dependence in the context of the multigluon distributions.

It is more appropriate to use the parton distributions unintegrated over the transverse momentum k_t in the framework of k_t -factorization QCD approach for semi-inclusive processes (such as inclusive jet production in DIS, electroweak boson production, etc.) at high energies. The k_t -factorization formalism provides solid theoretical grounds for the effects of initial gluon radiation and intrinsic parton transverse momentum k_t . The unintegrated gluon $f(x, k_t^2)$ distribution is directly related to the dipole-nucleon cross section, that is saturated at low Q or large transverse distances $r \sim 1/Q$ between quark q and antiquark \bar{q} in the $q\bar{q}$ dipole created from the splitting of the virtual photon γ^* in the ep DIS. Indeed, the suitable factorization approach in DIS (where $W \gg Q \gg \Lambda_{\text{QCD}}$) is provided by k_t -factorization [5].

The UGD, in its original definition, obeys the BFKL evolution equation in the x variable and being a nonperturbative quantity. To realistically describe the structure of the proton, we must introduce a k_t unintegrated gluon density, whose evolution at small- x is governed by the BFKL equation [6]. The object of the BFKL evolution equation at very

*Electronic address: boroun@razi.ac.ir

small x is the differential gluon structure function¹ of proton

$$f(x, k_t^2) = \frac{\partial xg(x, \mu^2)}{\partial \ln \mu^2} \Big|_{\mu^2=k_t^2} \quad (1)$$

which emerges in the color dipole picture (CDP) of inclusive deep inelastic scattering (DIS) and diffractive DIS into dijets [7]. Unintegrated distributions are required to describe measurements where transverse momenta are exposed explicitly.

The unintegrated gluon distribution function satisfies the BFKL equation for an alternative derivation in terms of color dipoles. The BFKL equation at leading order is given by

$$\frac{\partial f(x, k_t^2)}{\partial \ln(1/x)} = \int dk_t'^2 K(k_t^2, k_t'^2) f(x, k_t'^2), \quad (2)$$

which describes the evolution in $\ln(1/x)$ of the unintegrated gluon density and K is the BFKL kernel [2,3]. In the small x limit this basically gives a power law behavior in x ,

$$f(x, k_t^2) \sim h(k_t^2) x^{-\lambda}, \quad (3)$$

where $h \sim (k_t^2)^{-\frac{1}{2}}$ at large k_t^2 and λ is the maximum eigenvalue of the kernel K of the BFKL equation. For fixed α_s , λ has the value $\lambda = \frac{\alpha_s}{\pi} 12 \ln 2$, where this hard Pomeron has been termed the BFKL Pomeron and lead to very steeply rising V^*N cross-sections. In the BFKL analysis, there are infra-red (IR) and ultra-violet (UV) cutoffs on the k_t^2 integrations. Indeed determining the IR cutoff parameter is important for the integrating $\int dk_t^2 \alpha_s(k_t^2)$ down to $k_t^2 = 0$, also the choice of the UV cutoff is important when working at finite order² [8,9].

The color dipole picture (CDP) [10] has been introduced to study a wide variety of small x inclusive and diffractive processes at HERA. The CDP, at small x , gives a clear interpretation of the high-energy interactions, where is characterized by high gluon densities because the proton structure is dominated by dense gluon systems [11-13] and predicts that the small x gluons in a hadron wavefunction should form a Color Glass Condensate [14]. Dipole representation provides a convenient description of DIS at small x . There, the scattering between the virtual photon γ^* and the proton is seen as the color dipole where the transverse dipole size r and the longitudinal momentum fraction z with respect to the photon momentum are defined. The amplitude for the complete process is simply the production of these subprocess amplitudes, as the DIS cross section is factorized into a light-cone wave function and a dipole cross section. Using the optical theorem, this leads to the following expression for the γ^*p cross-sections

$$\sigma_{L,T}^{\gamma^*p}(x, Q^2) = \int dz d^2 \mathbf{r} |\Psi_{L,T}(\mathbf{r}, z, Q^2)|^2 \sigma_{\text{dip}}(x, \mathbf{r}), \quad (4)$$

where subscripts L and T referring to the transverse and longitudinal polarization state of the exchanged boson. Here $\Psi_{L,T}$ are the appropriate spin averaged light-cone wave functions of the photon and $\sigma_{\text{dip}}(x, r)$ is the dipole cross-section which related to the imaginary part of the $(q\bar{q})p$ forward scattering amplitude. The variable z , with $0 \leq z \leq 1$, characterizes the distribution of the momenta between quark and antiquark. The square of the photon wave function describes the probability for the occurrence of a $(q\bar{q})$ fluctuation of transverse size with respect to the photon polarization.

Another framework which can be used for calculating the parton distributions is based on the DGLAP evolution [15]. Deep inelastic electron-proton scattering is described in terms of scale dependent parton densities $q(x, \mu^2)$ and $g(x, \mu^2)$ [16], where the integrated gluon distribution ($xg(x, \mu^2)$) is defined through the unintegrated gluon distribution ($f(x, k_t^2)$) by

$$xg(x, \mu^2) \equiv \int^{\mu^2} \frac{dk_t^2}{k_t^2} f(x, k_t^2). \quad (5)$$

The unintegrated gluon distribution is related to the dipole cross section [4, 17]

$$\sigma(x, \mathbf{r}) = \frac{8\pi^2}{N_c} \int \frac{dk_t}{k_t^3} [1 - J_0(k_t \mathbf{r})] \alpha_s f(x, k_t^2). \quad (6)$$

¹ Eq.(1) is modified with the Sudakov form factor as x increase.

² This is the reason for applying that the DGLAP formulation ensures energy conservation order by order, but the BFKL formulation does not [2,3].

A novel formulation of the UGD for DIS in a way that accounts for the leading powers in both the Regge and Bjorken limits is presented in Ref.[18]. In this way, the UGD is defined by an explicit dependence on the longitudinal momentum fraction x which entirely spans both the dipole operator and the gluonic Parton Distribution Function (PDF).

In addition to the gluon momentum derivative model (i.e., Eq.(1)), several other models [7,10, 19-21] for the UGD have also been proposed so far. A comparison between these models can be found in Refs.[22,23]. The authors in Ref. [19] presented an x -independent model (ABIPSW) of the UGD where merely coincides with the proton impact factor by the following form

$$f(x, k_t^2) = \frac{A}{4\pi^2 M^2} \left[\frac{k_t^2}{M^2 + k_t^2} \right], \quad (7)$$

where M is a characteristic soft scale and A is the normalisation factor.

The authors in Ref. [7] presented a UGD soft-hard model (IN) in the large and small k_t regions by the following form

$$f(x, k_t^2) = f_{\text{soft}}^{(B)}(x, k_t^2) \frac{k_s^2}{k_s^2 + k_t^2} + f_{\text{hard}}(x, k_t^2) \frac{k_t^2}{k_h^2 + k_t^2}, \quad (8)$$

where the soft and the hard components are defined in [7].

The UGD model was considered in [20] to be used in the study of DIS structure functions and takes the form of a convolution between the BFKL gluon Green's function and a leading-order (LO) proton impact factor, where has been employed in the description of single-bottom quark production at LHC and to investigate the photoproduction of J/Ψ and Υ , by the following form (HSS model)

$$f(x, k_t^2, M_h) = \int_{-\infty}^{+\infty} \frac{d\nu}{2\pi^2} \mathcal{C} \frac{\Gamma(\delta - i\nu - \frac{1}{2})}{\Gamma(\delta)} \left(\frac{1}{x}\right)^{\chi(\frac{1}{2} + i\nu)} \left(\frac{k_t^2}{Q_0^2}\right)^{\frac{1}{2} + i\nu} \left\{ 1 + \frac{\bar{\alpha}_s^2 \beta_0 \chi_0(\frac{1}{2} + i\nu)}{8N_c} \log\left(\frac{1}{x}\right) \right. \\ \left. \times \left[-\psi\left(\frac{1}{2} + i\nu\right) - \log\left(\frac{k_t^2}{M_h^2}\right) \right] \right\}, \quad (9)$$

where $\chi_0(\frac{1}{2} + i\nu)$ and $\chi(\gamma)$ are respectively the LO and the next-to-leading order (NLO) eigenvalues of the BFKL kernel and $\beta_0 = 11 - \frac{2}{3}n_f$ with n_f the number of active quarks. Here $\bar{\alpha}_s = \frac{3}{\pi}\alpha_s(\mu^2)$ with $\mu^2 = Q_0 M_h$ where M_h plays the role of the hard scale which can be identified with the photon virtuality, $\sqrt{Q^2}$.

The authors in Ref. [21] presented a UGD model (Watt-Martin-Ryskin (WMR) model) where depends on an extra-scale μ , fixed at Q , by the following form

$$f(x, k_t^2, \mu^2) = T_g(k_t^2, \mu^2) \frac{\alpha_s(k_t^2)}{2\pi} \int_x^1 dz \left[\sum_q P_{gq}(z) \frac{x}{z} q\left(\frac{x}{z}, k_t^2\right) + P_{gg}(z) \frac{x}{z} g\left(\frac{x}{z}, k_t^2\right) \Theta\left(\frac{\mu}{\mu + k_t} - z\right) \right], \quad (10)$$

where $T_g(k_t^2, \mu^2)$ gives the probability of evolving from the scale k_t to the scale μ without parton emission and P_{ij} s are the splitting functions.

Golec-Biernat-Wusthoff (GBW) [10] presented a UGD model where derives from the effective dipole cross section $\sigma(x, \mathbf{r})$ for the scattering of a $q\bar{q}$ pair of a nucleon as³

$$f(x, k_t^2) = k_t^4 \sigma_0 \frac{R_0^2(x)}{2\pi} e^{-k_t^2 R_0^2(x)}, \quad (11)$$

with $R_0^2(x) = \frac{1}{\text{GeV}^2} \left(\frac{x}{x_0}\right)^{\lambda_p}$ and the following values $\sigma_0 = 23.03$ mb, $\lambda_p = 0.288$ and $x_0 = 3.04 \times 10^{-4}$. Although one of them (the HSS one) was fitted to reproduce DIS structure functions, the study of other reactions has provided an evidence that the UGD is not yet well known. The HSS model also reproduces well the forward Drell-Yan data at the LHC without any further adjustment of extra parameters [24]. In this paper we use the DGLAP-improved saturation model with respect to the UGD in the proton to access the dipole cross section at low x .

³ The reader can be referred to Refs.[7,10, 19-21] for a meticulous treatment of the parameters.

II. Method

The interaction of the $q\bar{q}$ pair with the proton is described by the dipole cross section. It is related to the gluon density in the target by the k_T -factorization formula [7,10,17]

$$\sigma(x, r) = \int \frac{d^2 k_t}{k_t^4} \frac{\partial x g(x, k_t^2)}{\partial \ln k_t^2} [1 - e^{i\mathbf{k}_t \cdot \mathbf{r}}][1 - e^{-i\mathbf{k}_t \cdot \mathbf{r}}], \quad (12)$$

where the relation between $f(x, k_t^2)$ and $xg(x, k_t^2)$ defined through Eq.(1).

• The DGLAP singlet evolution equation can be defined by considering the variable definitions $v \equiv \ln(1/x)$ and $w \equiv \ln(1/z)$, by the following form

$$\frac{\partial \widehat{\mathcal{F}}_2(v, k_t^2)}{\partial \ln k_t^2} = \int_0^v [\widehat{\mathcal{F}}_2(v, k_t^2) \widehat{\mathcal{H}}_{2,s}^{(\varphi)}(a_s(k_t^2), v-w) + \langle e^2 \rangle \widehat{\mathcal{G}}(v, k_t^2) \widehat{\mathcal{H}}_{2,g}^{(\varphi)}(a_s(k_t^2), v-w)] dw, \quad (13)$$

where $\langle e^2 \rangle$ is the average of the charge e^2 for the active quark flavors n_f , $\langle e^2 \rangle = n_f^{-1} \sum_{i=1}^{n_f} e_i^2$ and

$$\frac{\partial \widehat{\mathcal{F}}_2(v, k_t^2)}{\partial \ln k_t^2} \equiv \frac{\partial F_2(e^{-v}, k_t^2)}{\partial \ln k_t^2}, \quad \widehat{\mathcal{G}}(v, k_t^2) \equiv xg(e^{-v}, k_t^2), \quad \widehat{\mathcal{H}}^{(\varphi)}(a_s(k_t^2), v) \equiv e^{-v} \widehat{P}_{a,b}^{(\varphi)}(a_s(k_t^2), v). \quad (14)$$

The splitting function reads

$$P_{a,b}^{(\varphi)}(a_s, x) = \sum_{\phi=0}^{\varphi} a_s^{\phi+1}(k_t^2) P_{a,b}^{(\phi)}(x), \quad (15)$$

where ϕ denotes the order in running coupling $\alpha_s(k_t^2)$ and $a_s(k_t^2) = \alpha_s(k_t^2)/4\pi$. The Laplace transform of $\widehat{\mathcal{H}}(a_s(k_t^2), v)$'s are given by the following forms

$$\begin{aligned} \Phi_f^{(\varphi)}(a_s(k_t^2), s) &\equiv \mathcal{L}[\widehat{\mathcal{H}}_{2,s}^{(\varphi)}(a_s(k_t^2), v); s] = \int_0^\infty \widehat{\mathcal{H}}_{2,s}^{(\varphi)}(a_s(k_t^2), v) e^{-sv} dv, \\ \Theta_f^{(\varphi)}(a_s(k_t^2), s) &\equiv \mathcal{L}[\widehat{\mathcal{H}}_{2,g}^{(\varphi)}(a_s(k_t^2), v); s] = \int_0^\infty \widehat{\mathcal{H}}_{2,g}^{(\varphi)}(a_s(k_t^2), v) e^{-sv} dv. \end{aligned} \quad (16)$$

We know that the Laplace transforms of the convolution factors are simply the ordinary products of the Laplace transforms of the factors. Therefore, Eq.(13) in the Laplace space s reads as

$$\frac{\partial f_2(s, k_t^2)}{\partial \ln k_t^2} = \Phi_f^{(\varphi)}(a_s(k_t^2), s) f_2(s, k_t^2) + \langle e^2 \rangle \Theta_f^{(\varphi)}(a_s(k_t^2), s) xg(s, k_t^2), \quad (17)$$

where

$$\mathcal{L}[\widehat{\mathcal{F}}_2(v, k_t^2); s] = f_2(s, k_t^2), \quad \mathcal{L}[\widehat{\mathcal{G}}(v, k_t^2); s] = xg(s, k_t^2). \quad (18)$$

The gluon distribution into the parametrization of the proton structure function and its derivative with respect to $\ln k_t^2$ in s -space in Eq.(17) is given by the following form

$$xg(s, k_t^2) = k^{(\varphi)}(a_s(k_t^2), s) Df_2(s, k_t^2) - h^{(\varphi)}(a_s(k_t^2), s) f_2(s, k_t^2), \quad (19)$$

where

$$\begin{aligned} Df_2(s, k_t^2) &= \partial f_2(s, k_t^2) / \partial \ln k_t^2, \\ k^{(\varphi)}(a_s(k_t^2), s) &= 1 / (\langle e^2 \rangle \Theta_f^{(\varphi)}(a_s(k_t^2), s)), \\ h^{(\varphi)}(a_s(k_t^2), s) &= \Phi_f^{(\varphi)}(a_s(k_t^2), s) k^{(\varphi)}(a_s(k_t^2), s). \end{aligned}$$

The inverse Laplace transforms of Eq.(19) reads

$$\widehat{xg}^{(\varphi)}(v, k_t^2) \equiv \mathcal{L}^{-1}[xg(s, k_t^2); v] = \mathcal{L}^{-1}[k^{(\varphi)}(a_s(k_t^2), s) Df_2(s, k_t^2) - h^{(\varphi)}(a_s(k_t^2), s) f_2(s, k_t^2); v] \quad (20)$$

where the inverse transform of a product to the convolution of the original functions, giving

$$\mathcal{L}^{-1}[f(s) \times h(s); v] = \int_0^v \widehat{F}(w) \widehat{H}(v-w) dw.$$

The inverse Laplace transform of the functions k and h in Eq.(20) are defined by $\widehat{J}(v)$ and $\widehat{M}(v)$, as

$$\widehat{J}(v, k_t^2) \equiv \mathcal{L}^{-1}[k(s, k_t^2); v], \quad \widehat{M}(v, k_t^2) \equiv \mathcal{L}^{-1}[h(s, k_t^2); v]. \quad (21)$$

The functions k and h in s -space, into the Laplace transform of the splitting functions (P_{qq} and P_{qg}), are given by [25]

$$\begin{aligned} k^{(\phi)}(a_s(k_t^2), s) &= \left(\langle e^2 \rangle \mathcal{L}[e^{-v} \sum_{\phi=0}^1 a_s^{\phi+1}(k_t^2) \widehat{P}_{qq}^{(\phi)}(v); s] \right)^{-1}, \\ h^{(\phi)}(a_s(k_t^2), s) &= \frac{\mathcal{L}[e^{-v} \sum_{\phi=0}^1 a_s^{\phi+1}(k_t^2) \widehat{P}_{qg}^{(\phi)}(v); s]}{\langle e^2 \rangle \mathcal{L}[e^{-v} \sum_{\phi=0}^1 a_s^{\phi+1}(k_t^2) \widehat{P}_{qq}^{(\phi)}(v); s]}, \end{aligned} \quad (22)$$

where at small x , the kernels at NLO approximation in Eq.(16) are given by the following forms

$$\begin{aligned} \Theta_f(a_s, s) &\simeq 2n_f a_s \left[\frac{1}{1+s} - \frac{2}{2+s} + \frac{2}{3+s} \right] + a_s^2 C_A T_f \left[\frac{40}{9s} \right], \\ \Phi_f(a_s, s) &\simeq a_s \left[4 - \frac{8}{3} \left(\frac{1}{1+s} + \frac{1}{2+s} + 2S_1(s) \right) \right] + a_s^2 C_F T_f \left[\frac{40}{9s} \right], \end{aligned} \quad (23)$$

where $S_1(s) = \psi(s+1) + \gamma_E$, where $\psi(x)$ is the digamma function and $\gamma_E = 0.5772156\dots$ is Euler constant. Here $C_A = N_c = 3$, $C_F = \frac{N_c^2 - 1}{2N_c} = \frac{4}{3}$ and $T_f = \frac{1}{2}n_f$. The standard representation for QCD couplings in NLO (within the $\overline{\text{MS}}$ -scheme) approximation reads

$$\alpha_s^{\text{NLO}}(k_t^2) = \frac{4\pi}{\beta_0 \ln \frac{k_t^2}{\Lambda^2}} \left[1 - \frac{\beta_1}{\beta_0^2} \frac{\ln \ln \frac{k_t^2}{\Lambda^2}}{\ln \frac{k_t^2}{\Lambda^2}} \right], \quad (24)$$

where β_0 and β_1 are the one and two loop correction to the QCD β -function and Λ is the QCD cut-off parameter⁴. Therefore, the integrated gluon density is related to the proton structure function by the following form

$$xg^{(\varphi)}(x, k_t^2) = \int_x^1 \left[DF_2(\ln \frac{1}{y}, k_t^2) J(a_s(k_t^2), \ln \frac{y}{x}) - F_2(\ln \frac{1}{y}, k_t^2) M(a_s(k_t^2), \ln \frac{y}{x}) \right] \frac{dy}{y}, \quad (25)$$

where $F_2(x, k_t^2)$ is the proton structure function. The parametrization of F_2 in Ref.[26] has an expression for the asymptotic part of F_2 (no-valence) that accounts for the asymptotic behavior $F_2 \simeq \ln^2(1/x)$ at small x which describes fairly well the available experimental data on the reduced cross sections.

In next section we consider the UGD and the color dipole cross section due to the parametrization of the proton structure function in Eqs.(1) and (12) with respect to (25), respectively.

3. Numerical Results

The UGD is obtained directly in terms of the parameterization of the structure function $F_2(x, k_t^2)$ and its derivative. The resulting UGD with the k_t^2 -dependence due to the parametrization of the proton structure function are shown

⁴ The running coupling (24) is used in the evolution of the DGLAP equations. In the HSS approach, a running consistent with a global fit to jet observables was used to find the correct form for the DIS structure functions at small values of x in the full Q range [22]. In this regard, the infrared freezing of strong coupling at leading order (LO) is imposed by fixing $\Lambda_{QCD} = 200$ MeV as

$$\alpha_s(\mu^2) = \min \left\{ 0.82, \frac{4\pi}{\beta_0 \ln \left(\frac{\mu^2}{\Lambda_{QCD}^2} \right)} \right\}$$

in Fig. 1. In this figure, we plot the k_t^2 dependence of the UGD at $x = 10^{-3}$ and compared the unintegrated gluon distribution behavior due to the improved saturation model with the GBW model. An enhancement and then depletion is observable in the improved and GBW models. These picks occur at $k_t^2 \approx 10 \text{ GeV}^2$ and $k_t^2 \approx 1 \text{ GeV}^2$ in the improved and GBW models respectively. As we can see, the UGD behavior in the improved saturation model, in a wide range of k_t^2 , is softer than the GBW model. The error bands in Fig.1 in the improved saturation model are due to the uncertainties in the coefficients of the parametrization of the proton structure function.

In Fig. 2 we show the k_t distributions of three different unintegrated gluons at $x = 10^{-3}$. This figure compares

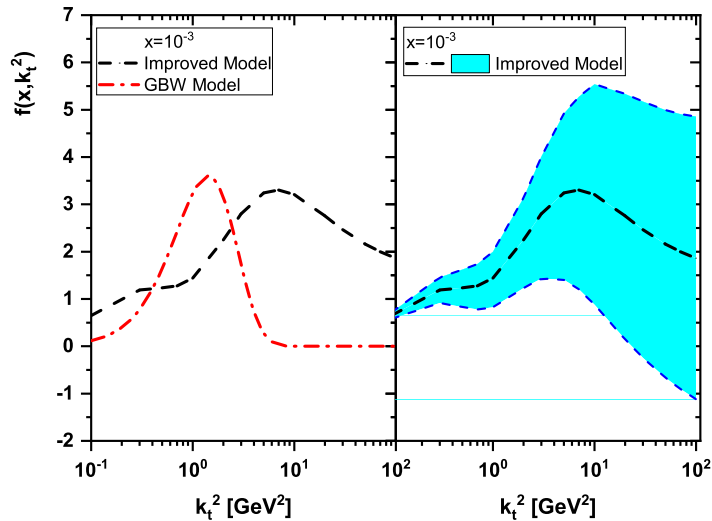


FIG. 1: Left: The UGD as a function of k_t^2 with respect to the improved model compared with the GBW model at $x = 10^{-3}$. Right: The error bands are due to the statistical uncertainties in the coefficients of the parametrization F_2 in [26].

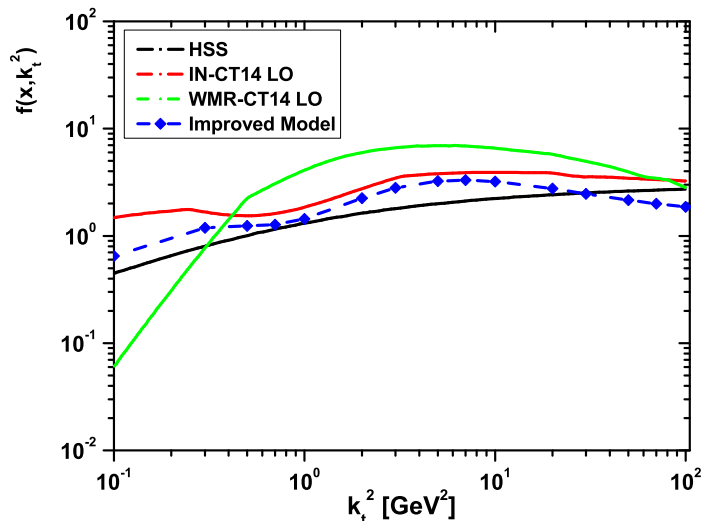


FIG. 2: The unintegrated gluon distribution $f(x, k_t^2)$ obtained from the improved saturation model (dashed-symbol), as a function of k_t^2 at $x = 10^{-3}$, compared with the HSS [20], IN [7] and WMR [21] models.

the results of the improved saturation model, based on the parametrization of the proton structure function, with the HSS [20], IN [7] and WMR [21] models. We observe that the improved saturation result is comparable with the

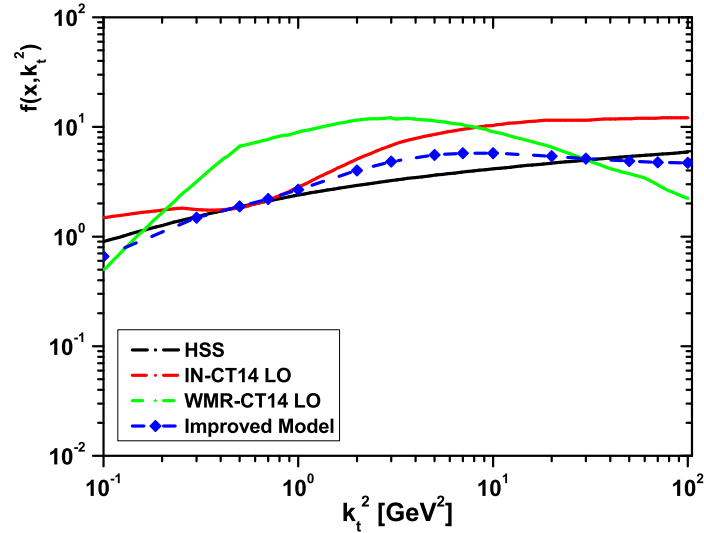


FIG. 3: The same as Fig.2 for $x = 10^{-4}$.

HSS and IN models in a wide range of k_t^2 . The differences are not large, however there is some suppression due to the models at large and small values of k_t^2 . The continuous behavior of the UGD in our model with increases of k_t^2 is due to the gluon and quark terms included in the improved saturation model.

In Fig.3 we present the unintegrated gluons with the k_t^2 -dependence of all the considered UGD models in Fig.2, for

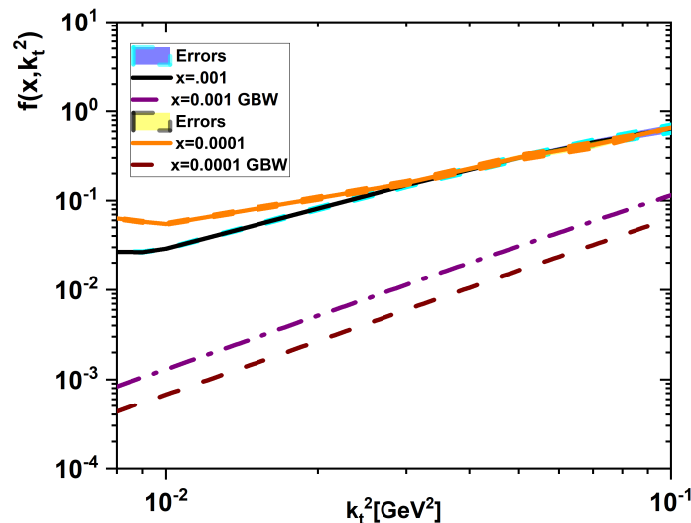


FIG. 4: Low k_t^2 -behavior of the considered UGD model for $x = 10^{-3}$ and 10^{-4} , as accompanied with the statistical uncertainties from the coefficients of the parameterization of F_2 in [26], compared with the GBW model (dashed and dashed-dot curves) [10].

$x = 10^{-4}$. The plot clearly shows the same behavior in the k_t^2 -shape of the figures at low values of x . In conclusion, the consistency of the several UGDs in their k_t dependence holds for values of $x = 10^{-3}$ and 10^{-4} in a wide range of k_t . Calculation of the dipole cross section requires the knowledge of the unintegrated gluon density for all scales

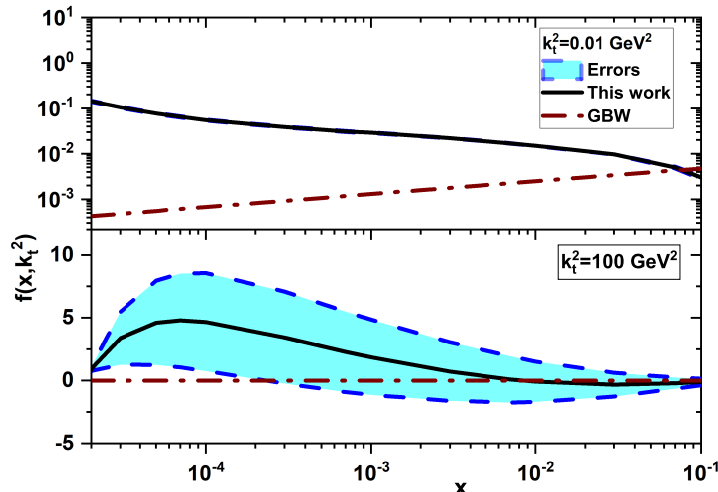


FIG. 5: x -behavior of the considered UGD model for $k_t^2 = 0.01 \text{ GeV}^2$ (up) and $k_t^2 = 100 \text{ GeV}^2$ (down), as accompanied with the statistical uncertainties from the coefficients of the parameterization of F_2 in [26], compared with the GBW model (dashed-dot curves) [10].

$0 < k_t^2 < \infty$. Usually the unintegrated gluon density is known for $k_t^2 > k_{t0}^2$ ($k_{t0}^2 = 1 \text{ GeV}^2$), so it is interesting to consider the function $f(x, k_t^2)$ for lowest values of $k_t^2 < k_{t0}^2$. Figure (4) illustrates the unintegrated gluon distributions $f(x, k_t^2)$ at low k_t^2 ($10^{-2} \text{ GeV}^2 \lesssim k_t^2 \leq 10^{-1} \text{ GeV}^2$). It shows that the modified UGD is different from the original GBW UGD at $k_t^2 \lesssim 10^{-2} \text{ GeV}^2$ and it is similar to the GBW UGD at $k_t^2 > 10^{-2} \text{ GeV}^2$ with a higher rate. In this range, the difference between the GBW UGD, for two different values of the longitudinal momentum fraction, $x = 10^{-3}$ and 10^{-4} is uniform, while they coincide with the improved UGD for $3 \times 10^{-2} \text{ GeV}^2 \lesssim k_t^2 \leq 10^{-1} \text{ GeV}^2$. These models in Fig.4 fairly reflect the distinct approaches whence each UGD descends in the range $3 \times 10^{-2} \text{ GeV}^2 \lesssim k_t^2 \leq 10^{-1} \text{ GeV}^2$. In Fig.5 we investigate the effect of different values of k_t^2 on the unintegrated gluon distribution in a wide range of x and compared with the GBW UGD model. We observe that the result for low k_t^2 (i.e., $k_t^2 = 0.01 \text{ GeV}^2$) is different with the GBW UGD model in the range $x < 0.1$. The difference between the results increases as x decreases. In particular the sensitivity of the predictions to a detailed parametrization of the infrared region which satisfies the gauge invariance constraints as $k_t^2 \rightarrow 0$ is considered. The uncertainties due to the statistical errors of the parametrization model are very small for low k_t^2 . These uncertainties increase as k_t^2 increase to 100 GeV^2 . In Fig.5 (down figure) we compare our results with the GBW UGD model at $k_t^2 = 100 \text{ GeV}^2$. The behavior of the GBW UGD model is uniform in a wide range of x and it is almost zero in this range. Our results has a fluctuation in the region $10^{-5} < x < 10^{-3}$ where this is the largest discrepancy is observed. This is due to the fact that as the gluon momentum fraction x decreases, the probability of the gluon splitting increases. One can see that the improved UGD is different from the GBW UGD at $10^{-5} < x < 10^{-3}$ and coincides with it at larger x ($10^{-3} < x < 10^{-1}$). Indeed, we have shown that our UGD is similar to the GBW UGD, obtained at large k_t (within the uncertainties) and different from it at low k_t in a wide range of x .

In Fig.6, we have calculated the improved saturation model with respect to the unintegrated gluon distribution to the ratio $\sigma_{\text{dip}}/\sigma_0$ in a wide range of the dipole size at the NLO approximation. Results of calculations and comparison with the GBW model [10] for $x = 10^{-3}$ and 10^{-4} are presented in figures 6 and 7, respectively. The effective parameters in the GBW model have been extracted from a fit of the HERA data as $\lambda = 0.288$ and $x_0 = 3.04 \times 10^{-4}$. These corrections to the ratio of color dipole cross sections at NLO approximation are comparable with the GBW model. For $rQ_s \geq 1$, the dashed curve (central values) merge due to geometric scaling in the dipole cross section in this region. In the right-hand of Figs.6 and 7, a particular interests present the ratio $\sigma_{\text{dip}}/\sigma_0$ defined by the scaling variable rQ_s , which means that the scattering amplitude and corresponding cross sections can scale on the dimensionless scale rQ_s . In conclusion, we observe that the geometric scaling holds for other values of x in a wide range of rQ_s . We observe that its violation for $rQ_s < 1$ is visible as x decreases.

In summary, we study the unintegrated gluon distribution from a parameterization of the proton structure function. In this analysis we present the k_t^2 -dependence of the improved UGD model at the NLO approximation

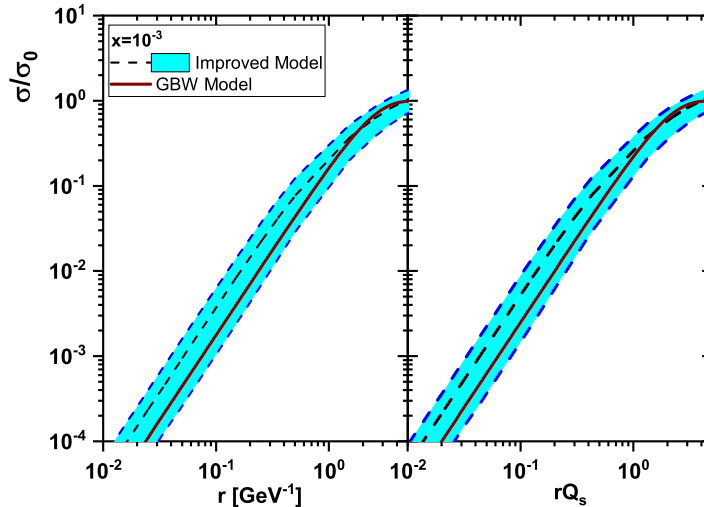


FIG. 6: The ratio of the dipole cross sections in the improved saturation model (dashed lines) as a function of r (left plot) and rQ_s (right plot) for $x = 10^{-3}$ at the NLO approximation. The solid lines are due to the GBW model [10]. The error bands are due to the statistical uncertainties from the coefficients of the parameterization of F_2 in [26].

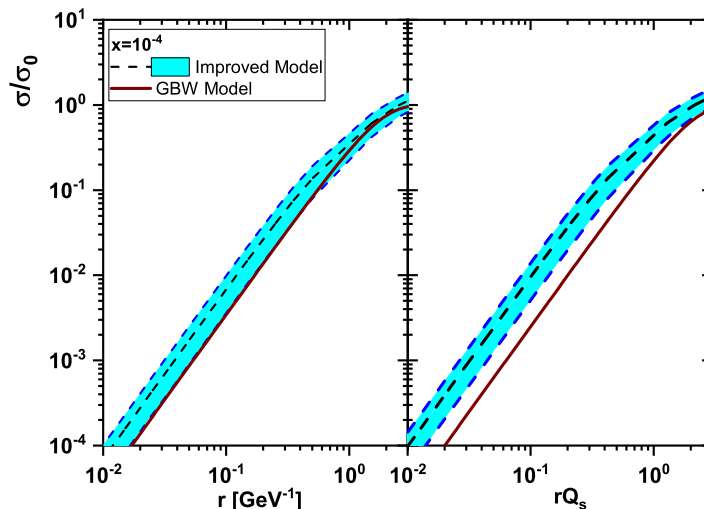


FIG. 7: The same as Fig.6 for $x = 10^{-4}$.

and compare with four models for $f(x, k_t^2)$, which exhibit rather different shape of k_t -dependence in the region, $10^{-1} \leq k_t^2 \leq 10^2$ GeV², for a value of the longitudinal momentum fraction, $x = 10^{-3}$. We show the behaviour of our predictions for the UGD are comparable with HSS and IN models in a wide range of k_t^2 . These results are comparable with the WMR and GBW models at moderate values of k_t^2 . It was shown that the improved UGD is different from the GBW UGD at low k_t and it coincides with the GBW UGD at large k_t .

Then we have presented the improved dipole cross section when the unintegrated gluon distribution is derived from the parametrization of the proton structure function as a function of r and rQ_s , respectively. The results according to the UGD are consistent with the GBW saturation model at the NLO approximation. The error bars are due to the statistical uncertainties of the effective parameters and preserved that the NLO results give a reasonable data description in comparison with the GBW model. In this method, the large dipole size part of the dipole cross section retains the features of the GBW model with the saturation scale. The dipole cross section at the small dipole size by the presence of

the unintegrated gluon distribution is modified in comparison with the saturation scale of the GBW saturation model.

ACKNOWLEDGMENTS

The author is grateful to Razi University for the financial support of this project. I am also very grateful to the respectable reviewer of the *Eur.Phys.J.C* **82**, 740(2022) article for suggesting this topic. Thanks also go to Z.Asadi for help with preparation of the UGD model.

REFERENCES

1. V.S.Fadin, E.A.Kuraev and L.N.Lipatov, *Phys.Lett.B* **60**, 50(1975); L.N.Lipatov, *Sov.J.Nucl.Phys.* **23**, 338(1976); I.I.Balitsky and L.N.Lipatov, *Sov.J.Nucl.Phys.* **28**, 822(1978).
2. G.Dissertori, I.G.Knowles and M.Schmelling, *Quantum Chromodynamics High Energy Experiments and Theory*, Oxford University Press, 2009; R.K.Ellis, W.J.Stirling and B.R.Webber, *QCD and Collider Physics*, Cambridge University Press, 1996.
3. A.M.Cooper-Sarkar, R.C.E.Devenish and A. De Roeck, *Int.J.Mod.Phys.A* **13**, 3385 (1998).
4. K.Kutak and A.M.Stasto, *Eur.Phys.J.C* **41**, 343 (2005).
5. G.I.Lykasov, A.A.Grinyuk and V.A.Bednyakov, arXiv [hep-ph]:1301.5156.
6. A.D.Bolognino, F.G.Celiberto, M.Fucilla, Dmitry Yu. Ivanov, A.Papa, W.Schafer and A.Szczurek, arXiv[hep-ph]:2202.02513.
7. I.P.Ivanov and N.N.Nikolaev, *Phys.Rev.D* **65**, 054004 (2002).
8. J.Kwiecinski, A.D.Martin and P.J.Sutton, *Z.Phys.C* **71**, 585 (1996); Jeffrey R.Forshaw, P.N.Harriman and P.J.Sutton, *J.Phys.G* **19**, 1616 (1993).
9. A.J.Askew, J.Kwiecinski, A.D.Martin and P.J.Sutton, *Phys.Rev. D* **49**, 4402 (1994); E.Elias, K.Golec-Biernat and Anna M.Stasto, *JHEP* **01**, 141 (2018).
10. K.Golec-Biernat and M.Wüsthoff, *Phys. Rev. D* **59**, 014017 (1998); K. Golec-Biernat and S.Sapeta, *JHEP* **03**, 102 (2018).
11. J.Bartels, K.Golec-Biernat and H.Kowalski, *Phys. Rev. D* **66**, 014001 (2002).
12. B.Sambasivam, T.Toll and T.Ullrich, *Phys.Lett.B* **803**, 135277 (2020).
13. J.R.Forshaw and G.Shaw, *JHEP* **12**, 052 (2004).
14. E.Iancu, A.Leonidov and L.McLerran, *Nucl.Phys.A* **692**, 583 (2001); *Phys.Lett.B* **510**, 133 (2001); E.Iancu, K.Itakura and S.Munier, *Phys.Lett.B* **590**, 199 (2004).
15. Yu.L.Dokshitzer, *Sov.Phys.JETP* **46**, 641 (1977); G.Altarelli and G.Parisi, *Nucl.Phys.B* **126**, 298 (1977); V.N.Gribov and L.N.Lipatov, *Sov.J.Nucl.Phys.* **15**, 438 (1972).
16. M.A.Kimber, J.Kwiecinski, A.D.Martin and A.M.Stasto, *Phys.Rev.D* **62**, 094006 (2000).
17. N.N.Nikolaev and B.G.Zakharov, *Phys.Lett.B* **332**, 184 (1994); N. N. Nikolaev and W. Schäfer, *Phys. Rev. D* **74**, 014023 (2006).
18. R.Boussarie and Y.Mehtar-Tani, *Phys.Lett.B* **831**, 137125 (2022).
19. I.V. Anikin, A. Besse, D.Yu. Ivanov, B. Pire, L. Szymanowski and S. Wallon, *Phys. Rev. D* **84**, 054004 (2011).
20. M. Hentschinski, A. Sabio Vera and C. Salas, *Phys. Rev. Lett.* **110**, 041601 (2013).
21. G. Watt, A.D. Martin and M.G. Ryskin, *Eur. Phys. J. C* **31**, 73 (2003).
22. A.D.Bolognino, F.G.Celiberto, Dmitry Yu. Ivanov and A.Papa, arXiv [hep-ph]:1808.02958; arXiv [hep-ph]:1902.04520; arXiv [hep-ph]:1808.02395.
23. F.G.Celiberto, *Nuovo Cim. C* **42**, 220 (2019).
24. F.G.Celiberto, D. Gordo Gomez and A.Sabio Vera, *Phys.Lett.B* **786**, 201 (2018).
25. G.R.Boroun, *Eur.Phys.J.C* **82**, 740 (2022); G.R.Boroun, *Eur.Phys.J.C* **83**, 42 (2023).
26. M. M. Block, L. Durand and P. Ha, *Phys. Rev.D* **89**, no. 9, 094027 (2014).